CHEMISTRY OF MATERIALS
Article

*Chem. Mater.* **2010,** *22,* 6263–6271 6263
DOI:10.1021/cm101811g

# Microemulsions as Reaction Media for the Synthesis of Bimetallic Nanoparticles: Size and Composition of Particles

Luis M. Magno,*[,†] Wilfried Sigle,[‡] Peter A. van Aken,[‡] Daniel G. Angelescu,[§] and Cosima Stubenrauch[†,∥]

[†]*School of Chemical and Bioprocess Engineering, University College Dublin, Belfield, Dublin 4, Ireland,* [‡]*Max-Planck-Institut für Metallforschung, Heisenbergstrasse 3, 70569 Stuttgart, Germany,* [§]*Institute of Physical Chemistry, I.G. Murgulescu Romanian Academy, 060021 Bucharest, Romani, and* [∥]*Institut für Physikalische Chemie, Universität Stuttgart, Pfaffenwaldring 55, 70569 Stuttgart, Germany*

*Received June 29, 2010. Revised Manuscript Received October 26, 2010*

This paper describes the synthesis of intermetallic Pt/Bi and Pt/Pb nanoparticles (NPs) using water-in-oil (w/o) microemulsions ($\mu$e) as template. For that purpose, w/o-microemulsions containing $H_2PtCl_6$+ $Pb(NO_3)_2$ and $H_2PtCl_6$+$Bi(NO)_3$, respectively, were mixed either with a w/o-microemulsion containing the reducing agent ($NaBH_4$) or with solid $NaBH_4$. A variation of the amount of reducing agent led to different particle compositions and sizes, while different ratios of the two metal salts only affected the composition but not the size of the resulting NPs. The size and structure of the microemulsion droplets were studied via small angle X-ray scattering (SAXS), and the intermetallic NPs were characterized by high resolution transmission electron microscopy (HRTEM) in combination with energy dispersive X-ray spectroscopy (EDX) and selected area electron diffraction (SAED). The results revealed that it is indeed possible to synthesis Pt/Pb and Pt/Bi intermetallic nanoparticles of ∼3−8 nm in diameter at low temperatures.

## 1. Introduction

Nanostructured materials can have unique electronic, magnetic, and catalytic properties. Great emphasis has been placed on the development of templates for the synthesis of nanostructured particles. The presence of more than one compound in the metallic nanoparticles is of particular interest since the physical and chemical interactions between different atoms can lead to new properties. For example, it turned out that combining a transition metal with platinum enhances the catalytic activities for reactions such us oxygen reduction in fuel cells and direct oxidation of methanol as compared to the pure Pt catalyst.[1,2] Recently, ordered intermetallic compounds such as Pt/Bi and Pt/Pb have emerged as a new kind of electrocatalyst.[3,4] Ordered intermetallic compounds are mixtures of two (or more) metals with a specific lattice structure, which differs from those of its constituent metals. [Note that the lattice structure of an alloy is the same as that of its main compound. All other metal atoms are either placed in the interstices of the host (interstitial alloy) or they replace atoms of the host metal (substitutional alloy).[5]]. One of the challenges in the synthesis of intermetallic nanoparticles is the fact that the respective compounds can have very different reduction potentials. For example, it holds for the metal salts of the compounds mentioned above that $[PtCl_6]^{2-}/[PtCl_4]^{2-} = +0.68$ V, $[PtCl_4]^{2-}/Pt = +0.76$ V, $Bi^{3+}/Bi = +0.22$ V, and $Pb^{2+}/Pb = -0.13$ V. Moreover, most reducing agents have low water stability. Thus, introducing new routes toward the synthesis of intermetallic nanoparticles in general and of intermetallic Pt/Bi and Pt/Pb nanoparticles in particular is of prime importance. Usually, intermetallic compounds are synthesized under extreme conditions, such as melting and long-time annealing at high temperatures.[3,4,6] However, the preparation of intermetallic nanoparticles under mild conditions is still a challenge. Solving this problem is important: It is expected that nanoparticles (NPs) synthesized at low temperatures with a narrow size distribution will have better catalytic activities than the current ones.[7,8]

A promising route to tackle this challenge is the use of microemulsions via which it is indeed possible to synthesize NPs with a narrow size distribution at low temperatures. So far, the microemulsion technique was pursued to prepare Pt-metal catalysts for oxygen reduction in fuel cells[7,9−14] as well as for the synthesis of bimetallic particles composed of metals with similar reduction potentials

(1) Watanabe, M.; Tsurumi, K.; Mizukami, T.; Nakamura, T.; Stonehart, P. *J. Electrochem. Soc.* **1994**, *141*(10), 2659–2668.
(2) Yohannes, T.; Inganas, O. *J. Electrochem. Soc.* **1996**, *143*(7), 2310–2314.
(3) Casado-Rivera, E.; Volpe, D. J.; Alden, L.; Lind, C.; Downie, C.; Vazquez-Alvarez, T.; Angelo, A. C. D.; DiSalvo, F. J.; Abruna, H. D. *J. Am. Chem. Soc.* **2004**, *126*(12), 4043–4049.
(4) Casado-Rivera, E.; Gál, Z.; Angelo, A. C.; Lind, C.; DiSalvo, F.; Abruña, H. *ChemPhysChem* **2003**, *4*(2), 193–199.
(5) West, A. R. *Basic Solid State Chemistry*, 2nd ed.; John Wiley and Sons: New York, 1999.
(6) Wang, H.; Alden, L.; DiSalvo, F. J.; Abruna, H. D. *Phys. Chem. Chem. Phys.* **2008**, *10*(25), 3739–3751.
(7) Escudero, M. J.; Hontañón, E.; Schwartz, S.; Boutonnet, M.; Daza, L. *J. Power Sources* **2002**, *106*(1−2), 206–214.
(8) Xiong, L.; Manthiram, A. *Electrochim. Acta* **2005**, *50*(11), 2323–2329.
(9) Sine, G.; Smida, D.; Limat, M.; Foti, G.; Ch, C. *J. Electrochem. Soc.* **2007**, *154*(2), B170–B174.
(10) Zhao, S.-Y.; Chen, S.-H.; Wang, S.-Y.; Li, D.-G.; Ma, H.-Y. *Langmuir* **2002**, *18*(8), 3315–3318.


Published on Web 11/15/2010

(e.g., Pt/Ag,[15] Pt/Au,[16] and Pt/Pd[17,18]). However, to the best of our knowledge, the synthesis of bimetallic particles with metals of largely different reduction potentials has not yet been achieved. Microemulsions are defined as isotropic, macroscopically homogeneous, and thermodynamically stable mixtures containing a polar phase such as water, a nonpolar phase such as oil, and a surfactant that forms an interfacial film separating the polar and nonpolar domains. Water-in-oil microemulsions contain nanometer-sized water droplets dispersed in an oil phase stabilized by the surfactant layer. The main advantage of the use of a water-in-oil microemulsion as reaction medium is the fact that the size and shape of the droplet sizes can be controlled by varying the temperature and composition of the microemulsion. For the synthesis of metallic nanoparticles, the metal source, e.g., a metal salt, is solubilized in the aqueous phase of a water-in-oil microemulsion, whereas the reducing agent, such as hydrazine or sodium borohydride, is added either as a solid compound[9,19,20] solubilized in a second water-in-oil microemulsion[21−26] or dissolved in a solvent [27][Excellent reviews of the synthesis of inorganic nanoparticles via microemulsions can be found in refs 22, 34, and 30.] In water-in-oil (w/o) microemulsions, an exchange between the aqueous phases of the two microemulsions occurs via a fusion−fission process[28] and the metal salt and reducing agent will eventually be distributed evenly throughout the aqueous phase. At the same time, the metal reduction will take place in the aqueous phase resulting in monodisperse inorganic nanoparticles.

With the final goal of synthesizing effective Pt/Pb and Pt/Bi catalysts for fuel cells, we developed and optimized the microemulsion technique. In our previous work, a systematic study on the influence of the metal salt(s) and the reducing agent, respectively, on the phase behavior of microemulsion was carried out.[29] The water emulsification failure boundaries (wefb) of all relevant systems were determined and "fine-tuned" by adding 1-octanol such that the wefbs of the two microemulsions match. In the present study, we report on the synthesis of Pt/Pb and Pt/Bi intermetallic particles. For that purpose, w/o-microemulsions containing $H_2PtCl_6 + Pb(NO_3)_2$ and $H_2PtCl_6 + Bi(NO)_3$, respectively, were mixed either with a w/o-microemulsion containing the reducing agent ($NaBH_4$) or with solid $NaBH_4$. The size of the templating w/o-microemulsions containing the metal salts and the reducing agent, respectively, as well as the time evolution of particle formation and the growth of the particles in the w/o-microemulsion pools were studied by small angle X-ray scattering (SAXS). The size distribution of the resulting particles was studied by transmission electron microscopy (TEM) analysis, while the particle composition and the respective crystal structures were investigated by high resolution transmission electron microscopy (HRTEM), selected area electron diffraction (SAED), and energy dispersive X-ray spectroscopy (EDX). We also report on the effect of the metal-to-salt ratio and the amount of reducing agent on the particle size and particle composition as well as on the effect of adding the reducing agent in a w/o-microemulsion compared to directly adding it as a solid.

## 2. Experimental Section

**2.1. Materials.** The oil *n*-octane (99.5%) was purchased from Fluka. The alcohol 1-octanol (99%) and the surfactant Brij30 were purchased from Sigma Aldrich. Brij30 contains an average of four ethylene oxide groups and a linear alkyl chain of $C_{12}H_{25}$. The metal salts hexachloroplatinic acid ($H_2PtCl_6 \cdot 6H_2O$, 99.9%), lead(II) nitrate ($Pb(NO_3)_2$, 99.999%), and bismuth(III) nitrate pentahydrate ($Bi(NO_3)_3 \times 5H_2O$, 99.999%) and the reducing agent sodium borohydride ($NaBH_4$, 99%) were also supplied by Sigma Aldrich. Ethoxylated polyethylene imine (PEI20EO) was supplied by BASF. All chemicals were used without further purification. The water used was treated with a Millipore-Q water purification system.

**2.2. Method for Nanoparticle Preparation.** The preparation of metallic nanoparticles (NPs) was carried out by mixing two different microemulsions that consisted of an aqueous solution, the oil *n*-octane, the surfactant Brij30, and the alcohol 1-octanol (route 1). The aqueous phase of one microemulsion contained metal salts, while the aqueous phase of the second microemulsion contained the reducing agent $NaBH_4$. In regards to the metal salts, either a mixture of $H_2PtCl_6$+$Pb(NO_3)_2$ or $H_2PtCl_6$+$Bi(NO_3)_3$ was chosen. Note that for the solubilization of $Bi(NO_3)_3$ in an aqueous solution 2 M $H_2NO_3$ needed to be added. The microemulsions which contained either the metal salts or the reducing agent were prepared at constant overall mass fraction of the aqueous phase ($w_A$), while they differed with respect to the composition of the aqueous phase and to the cosurfactant content. The latter was varied in order to obtain an overlap of the water emulsification failure boundary (wefb) of the two microemulsions.[29] Nitrogen was bubbled through all

(11) Godoi, D. R. M.; Perez, J.; Villullas, H. M. *J. Electrochem. Soc.* **2007**, *154*(5), B474–B479.
(12) Malheiro, A. R.; Varanda, L. C.; Perez, J.; Villullas, H. M. *Langmuir* **2007**, *23*(22), 11015–11020.
(13) Santos, L. G. R. A.; Oliveira, C. H. F.; Moraes, I. R.; Ticianelli, E. A. *J. Electroanal. Chem.* **2006**, *596*(2), 141–148.
(14) Magno, L. M.; Angelescu, D. G.; Sigle, W.; Stubenrauch, C. *Phys. Chem. Chem. Phys.* **2010**, DOI: 10.1039/C0CP01085E.
(15) Wu, M.-L.; Lai, L.-B. *Colloids Surf., A* **2004**, *244*(1−3), 149–157.
(16) Wu, M.-L.; Chen, D.-H.; Huang, T.-C. *Chem. Mater.* **2001**, *13*(2), 599–606.
(17) Yashima, M.; Falk, L. K. L.; Palmqvist, A. E. C.; Holmberg, K. *J. Colloid Interface Sci.* **2003**, *268*(2), 348–356.
(18) Wu, M.-L.; Chen, D.-H.; Huang, T.-C. *J. Colloid Interface Sci.* **2001**, *243*(1), 102–108.
(19) Rojas, S.; García-García, F. J.; Järas, S.; Martínez-Huerta, M. V.; Fierro, J. L. G.; Boutonnet, M. *Appl. Catal., A: Gen.* **2005**, *285*(1−2), 24–35.
(20) Solla-Gullón, J.; Vidal-Iglesias, F. J.; Montiel, V.; Aldaz, A. *Electrochim. Acta* **2004**, *49*(28), 5079–5088.
(21) Boutonnet, M.; Lögdberg, S.; Elm Svensson, E. *Curr. Opin. Colloid Interface Sci.* **2008**, *13*(4), 270–286.
(22) Ingelsten, H. H.; Bagwe, R.; Palmqvist, A.; Skoglundh, M.; Svanberg, C.; Holmberg, K.; Shah, D. O. *J. Colloid Interface Sci.* **2001**, *241*(1), 104–111.
(23) Pileni, M.-P. *Nat. Mater.* **2003**, *2*(3), 145–150.
(24) Wu, M.-L.; Chen, D.-H.; Huang, T.-C. *Langmuir* **2001**, *17*(13), 3877–3883.
(25) Naoe, K.; Petit, C.; Pileni, M. P. *Langmuir* **2008**, *24*(6), 2792–2798.
(26) Fang, J.; Stokes, K. L.; Wiemann, J. A.; Zhou, W. L.; Dai, J.; Chen, F.; O'Connor, C. J. *Mater. Sci. Eng. B* **2001**, *83*(1−3), 254–257.
(27) Calandra, P.; Giordano, C.; Longo, A.; Liveri, V. T. *Mater. Chem. Phys.* **2006**, *98*(2−3), 494–499.
(28) Capek, I. *Adv. Colloid Interface Sci.* **2004**, *110*(1−2), 49–74.
(29) Magno, M.; Angelescu, D. G.; Stubenrauch, C. *Colloids Surf., A* **2009**, *348*(1−3), 116–123.
(30) Mitchell, D. R. *Microsc. Res. Tech.* **2008**, *71*(8), 588–593.

**Table 1. Compositions of Samples and Preparation Temperature Used for the Synthesis of Bimetallic Nanoparticles at a Mass Fraction of the Aqueous Phase of $w_A = 0.08$[a]**

Pt/Pb Bimetallic Nanoparticles

| aqueous phase[b] | $\gamma_b$ | $\delta$ | $T_{wefb}$/°C | sample |
|---|---|---|---|---|
| 13 mM $H_2PtCl_6$/13 mM $Pb(NO_3)_2$ | 0.114 | 0.37 | 30.5 | 1a |
| 160 mM $NaBH_4$ | 0.095 | 0.22 | 30.5 | |
| 13 mM $H_2PtCl_6$/13 mM $Pb(NO_3)_2$ | 0.114 | 0.37 | 30.5 | 1b |
| 320 mM $NaBH_4$ | 0.095 | 0.22 | 29.5 | |
| 13 mM $H_2PtCl_6$/13 mM $Pb(NO_3)_2$ | 0.114 | 0.37 | 29.5 | 1c |
| 0.012 g $NaBH_4$ | | | | |
| 13 mM $H_2PtCl_6$/26 mM $Pb(NO_3)_2$ | 0.114 | 0.37 | 30.5 | 1d |
| 320 mM $NaBH_4$ | 0.095 | 0.22 | 30.5 | |
| 13 mM $H_2PtCl_6$/39 mM $Pb(NO_3)_2$ | 0.114 | 0.37 | 30.5 | 1e |
| 320 mM $NaBH_4$ | 0.095 | 0.22 | 30.5 | |

Pt/Bi Bimetallic Nanoparticles

| aqueous phase[b] | $\gamma_b$ | $\delta$ | $T_{wefb}$/°C | sample |
|---|---|---|---|---|
| 13 mM $H_2PtCl_6$/13 mM $Bi(NO_3)_3$ | 0.140 | 0.50 | 31.0 | 2a[c] |
| 160 mM $NaBH_4$ | 0.092 | 0.27 | 31.0 | |
| 13 mM $H_2PtCl_6$/13 mM $Bi(NO_3)_3$ | 0.140 | 0.50 | 30.0 | 2b[c] |
| 320 mM $NaBH_4$ | 0.092 | 0.27 | 30.0 | |
| 13 mM $H_2PtCl_6$/13 mM $Bi(NO_3)_3$ | 0.140 | 0.50 | 30.0 | 2c[c] |
| 0.012 g of $NaBH_4$ | | | | |

[a] $\gamma_b$ represents the mass fraction of Brij30 and 1-octanol in the oil phase. $\delta$ is the mass fraction of 1-octanol in the mixture of 1-octanol and Brij30. $T_{wefb}$ is the phase transition temperature between the 1- and $\overline{2}$-phase region. [b] $M_w(H_2PtCl_6) = 409.81\ g\ mol^{-1}$; $M_w(Pb(NO_3)_2) = 331.2\ g\ mol^{-1}$; $M_w(Bi(NO_3)_3) = 485.07\ g\ mol^{-1}$. [c] $N_2$ was bubbled through the solutions before, during, and after mixing them for ~30 min.

aqueous solutions (solutions containing metal salts or reducing agent) in order to prevent metal oxidation by $O_2$. In the case of the "Pt/Bi" samples, $N_2$ was bubbled not only through the aqueous solutions but also through the microemulsions before and after mixing them for about 30 min (see Table 1). The sample compositions are given by (1) the mass fraction of surfactant, Brij30 (C), and cosurfactant, 1-octanol (D), in oil (B)

$$\gamma_b = \frac{m_C + m_D}{m_B + m_C + m_D} \quad (1)$$

(2) the mass fraction of cosurfactant, 1-octanol (D), in the mixture of 1-octanol and Brij30

$$\delta = \frac{m_D}{m_C + m_D} \quad (2)$$

(3) the overall mass fraction of the aqueous phase (A) in the total system

$$w_A = \frac{m_A}{m_{total}} \quad (3)$$

Prior to any synthesis, the two microemulsions were equilibrated at the desired temperature for about half an hour, and then, they were combined by adding the metal-salt-containing microemulsion to the microemulsion containing the reducing agent via a single fast step under vigorous stirring. [Schmidt et al. reported that adding the metal-salt-containing microemulsion to the one that contains the reducing agent leads to a much narrower size distribution as compared to the opposite mixing protocol.[35]]. Metallic nanoparticles were also prepared by directly adding the reducing agent ($NaBH_4$) as a powder to the metal-salt-containing microemulsion at $T_{wefb}$ (route 2). Both processes immediately turned the solution a dark color. After mixing, the system was stirred for about 1 h at constant temperature. Thirty minutes later, 2 to 3 droplets of ethoxylated polyethylene imine (PEI20EO) were added to avoid particle agglomeration. The final products were collected by a centrifugation process and then washed successively by ethanol and acetone.

**2.3. Techniques for Nanoparticle Characterization.** For particle characterization, high-resolution transmission electron microscopy (HRTEM) images were collected on a JEOL 4000 EX (operated at 400 keV). Energy-dispersive X-ray analysis (EDX) was done on the Zeiss SESAM. Selected area electron diffraction (SAED) patterns were collected on the JEOL 4000 EX. All experiments were conducted at room temperature and ambient pressure. The nanoparticles were dissolved in ethanol and then deposited on thin holey carbon films (Plano, 300 mesh, *Artikel S147-3*). HRTEM images and SAED patterns were either recorded on a negative film (JEOL 4000 EX) which was digitalized using a negative scanner or directly recorded on a 2kx2k CCD camera (Gatan UltraScan; Zeiss SESAM). For data analysis, the Gatan DigitalMicrograph software was used. Lattice spacings were obtained from HRTEM images by linescans across lattice fringes. The diameter of diffraction rings was obtained using the DiffTools package.[30] For calibration, diffraction patterns of pure Si were used.

## 3. Results and Discussion

The size and composition of particles, which were prepared by mixing a microemulsion containing a mixture of two metal salts with a microemulsion containing the reducing agent (Table 1), were studied by TEM and EDX, respectively. In order to obtain complementary information on the crystal structure and the composition, SAED patterns were recorded and the data evaluated as described in ref 30. HRTEM was also used to identify the interplanar spacings of the crystal lattices presented in all samples. Note that with EDX the presence of oxygen was observed in all samples. However, it is neither possible to quantify the amount of oxygen nor to identify the oxygen source. Oxygen could come from $O_2$ adsorption on the Cu-grid, the formation of metal-oxides, or both.

**3.1. Pt/Pb Mixtures.** In the following, the influence of the $NaBH_4$ concentration and of the metal salt ratio ($H_2PtCl_6$/$Pb(NO_3)_2$) of the precursor microemulsions on the size and composition of the NPs will be discussed. The bimetallic Pt/Pb nanoparticles were prepared by route 1 and route 2 as described in Section 2.2. The TEM analysis of 60 particles selected randomly shows that the average diameter is 4.0 ± 1.0 nm for all samples prepared via route 1. Moreover, a uniform dispersion of spherical nanoparticles was observed for all samples. All particles presented in this section were prepared at $w_A = 0.08$, and small-angle X-ray scattering (SAXS) measurements revealed that the microemulsion droplets were indeed all spherical and of the same size, namely, 26.0 ± 2.0 nm (see Table S1 and Figure S1 in Supporting Information).

*3.1.1. Effect of Reducing Agent on Size and Composition of Pt/Pb Nanoparticles.* In order to study the influence of the $NaBH_4$ concentration on the synthesis of Pt/Pb

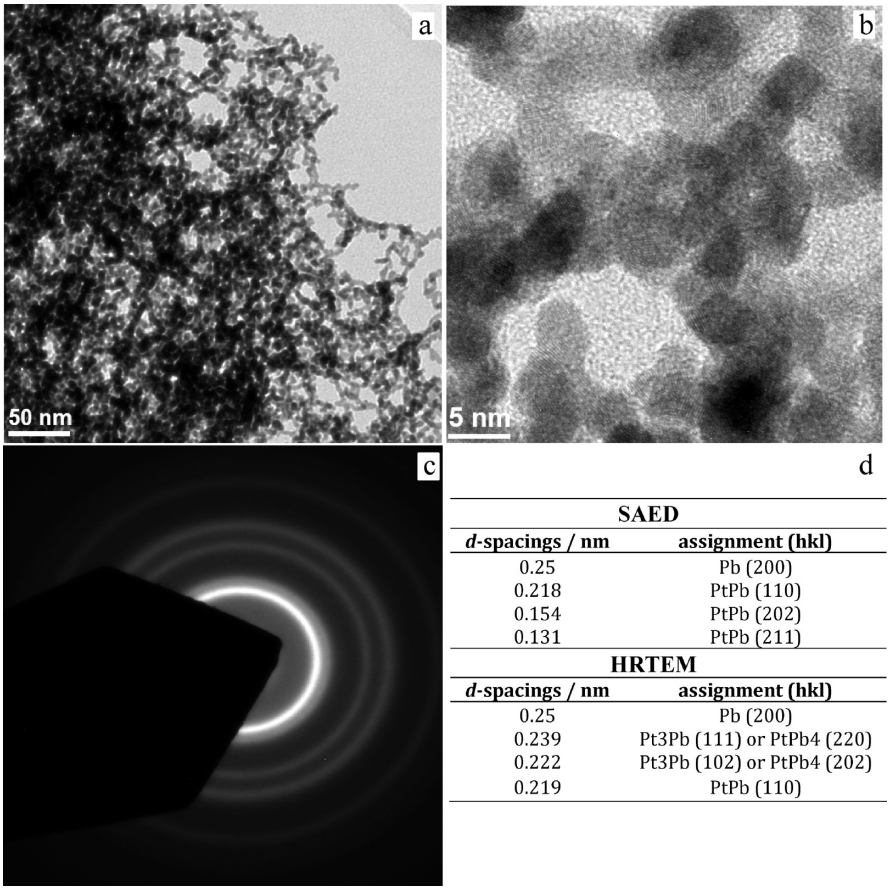


| SAED | |
|---|---|
| *d*-spacings / nm | assignment (hkl) |
| 0.25 | Pb (200) |
| 0.218 | PtPb (110) |
| 0.154 | PtPb (202) |
| 0.131 | PtPb (211) |
| **HRTEM** | |
| *d*-spacings / nm | assignment (hkl) |
| 0.25 | Pb (200) |
| 0.239 | Pt3Pb (111) or PtPb4 (220) |
| 0.222 | Pt3Pb (102) or PtPb4 (202) |
| 0.219 | PtPb (110) |

**Figure 1.** Characterization of sample 1a (13 mM $H_2PtCl_6$/13 mM $Pb(NO_3)_2$−160 mM $NaBH_4$) with (a) a bright-field TEM image of NPs, (b) a HRTEM image of NPs, (c) an electron diffraction pattern of the TEM image, and (d) a table with the *d*-spacings (nm) obtained from selected area electron diffraction (SAED) patterns and HRTEM analysis of sample 1a. SAED was measured in different areas of the sample (six different areas).

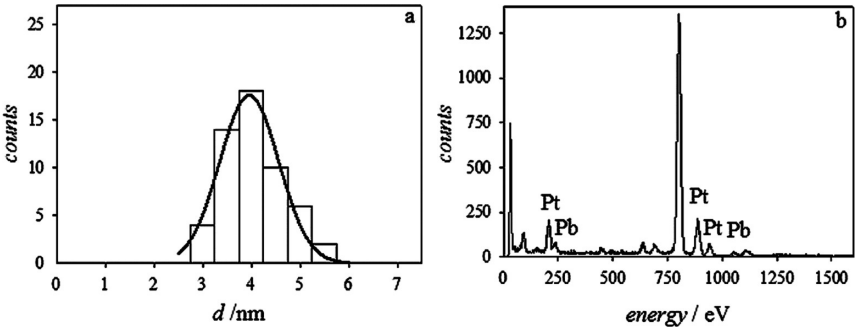


**Figure 2.** (a) Particle size (diameter *d*) distribution using a Gaussian fit of Pt/Pb NPs from sample 1a (4.0 ± 1.0 nm) and (b) EDX spectrum over 10 $nm^2$ area of sample 1a.

NPs, three samples were prepared at different reducing agent concentrations (samples 1a, 1b, and 1c) and at a 1:1 molar ratio of the two metal salts (13 mM $H_2PtCl_6$/13 mM $Pb(NO_3)_2$) as presented in Table 1. In sample 1a, particles were prepared via route 1 by combining a w/o-microemulsion containing a mixture of 13 mM $H_2PtCl_6$ and 13 mM $Pb(NO_3)_2$ with a w/o-microemulsion containing 160 mM $NaBH_4$. A TEM image, an HRTEM image, and an electron diffraction pattern are shown in Figure 1. The TEM analysis for 60 particles selected randomly shows that the average diameter is 4.0 ± 1.0 nm as shown in Figure 2a. The EDX analysis of different areas (5−200 $nm^2$) shows some regions that are rich in Pb (Pt/Pb atomic ratio of 10:90) and other regions with a Pt/Pb atomic ratio around 3:1 (see Figure 2b). The SAED measurement and the HRTEM analysis show the presence of various intermetallic phases, namely, $Pt_3Pb$, Pt/Pb, and $Pt/Pb_4$ in agreement with the phase diagram of the binary system Pt/Pb.[31] However, the presence of a $Pt/Pb_4$ phase cannot be clearly deduced from the SAED and HRTEM analysis. Also, the high Pt concentration measured in most areas by EDX does not suggest a large amount of $Pt/Pb_4$. Some diffraction patterns could be assigned to Pb so that the

(31) Hansen, M.; Anderko, K., *Constitution of Binary Alloys*, 2nd ed.; McGraw-Hill: New York, 1958.

formation of pure Pb cannot fully be ruled out. Thus, intermetallic phases are indeed formed, while no experimental evidence of a core−shell structure was found.

In sample 1b (13 mM $H_2PtCl_6$/13 mM $Pb(NO_3)_2$−320 mM $NaBH_4$), a higher concentration of reducing agent was used compared to sample 1a. The crystal *d*-spacings observed in the electron diffraction patterns indicate the coexistence of $Pt_3Pb$, Pt/Pb, and $Pt/Pb_4$ phases as shown in Table 2. The *d*-spacings observed by HRTEM are in good agreement with the SAED results (see Table 2). Complementary EDX analyses of different areas (5−200 $nm^2$) show again some regions that are rich in Pb (Pt/Pb atomic ratio of 10:90) as was the case for sample 1a and other regions with a Pt/Pb atomic ratio around 2:1, respectively (see Table S2 in Supporting Information). Comparing the atomic ratios of samples 1a and 1b (see Table S2 in Supporting Information), one can conclude that more of the Pb-rich phase $Pt/Pb_4$ is formed if one increases the $NaBH_4$ concentration, while the NP size is not affected, as mentioned above.

**Table 2. *d*-spacings from SAED Patterns and HRTEM Analysis of Sample 1b (13 mM $H_2PtCl_6$/13 mM $Pb(NO_3)_2$−320 mM $NaBH_4$)[a]**

| SAED | | | |
|---|---|---|---|
| *d*-spacings/nm | assignment (hkl) | *d*-spacings/nm | assignment (hkl) |
| 0.433 | | 0.433 | |
| 0.242 | Pb (200) | 0.321 | |
| 0.211 | Pt/Pb (102) | 0.279 | $Pt/Pb_4$ (211) |
| 0.148 | Pt/Pb (202), $Pt_3Pb$ (220), or $Pt/Pb_4$ (004) | 0.197 | $Pt_3Pb$ (200) |
| 0.127 | Pt/Pb (212), $Pt_3Pb$ (311), or $Pt/Pb_4$ (212) | 0.168 | $Pt/Pb_4$ (213) |

| HRTEM | |
|---|---|
| *d*-spacings/nm | assignment (hkl) |
| 0.306 | Pt/Pb (101) |
| 0.263 | $Pt/Pb_4$ (211) |
| 0.244 | $Pt/Pb_4$ (211) or Pb (200) |
| 0.237 | $Pt_3Pb$ (111) |
| 0.214 | Pt/Pb (110) |

[a] SAED was measured in different areas of the sample (six different areas), and two different diffraction patterns were obtained.

The bimetallic particles containing Pt and Pb were also prepared via route 2 by adding 0.012 g of $NaBH_4$ to the microemulsion containing 13 mM of $H_2PtCl_6$ and 13 mM $Pb(NO_3)_2$ (sample 1c) at $T_{wefb}$. In this case, the concentration of $NaBH_4$ is at least 2 times higher than the concentration used in sample 1b although it is hard to define the exact concentration per droplet as the $NaBH_4$ is added as a solid to the microemulsion containing the metal salts. The crystal *d*-spacings observed by HRTEM can be attributed to a Pt/Pb phase as can be seen in Table 3. Selected area electron diffraction (SAED) measurements over six different areas of the sample show again the presence of Pt/Pb, $Pt_3Pb$, and $Pt/Pb_4$ phases. Complementary EDX analyses of different areas (5−200 $nm^2$) show some regions that are rich in Pb (Pt/Pb atomic ratio of 10:90) and other regions with a Pt/Pb atomic ratio of around 2:1 and 3:1, respectively. These results suggest that a coexistence of $Pt_3Pb$, Pt/Pb, and $Pt/Pb_4$ was obtained as observed for sample 1b.

As can be seen in Figure 3, the TEM analysis of 60 particles selected randomly indicates a bimodal distribution of particles with an average diameter of $6.5 \pm 1.0$ and $9.0 \pm 1.5$ nm, respectively. Comparing these particles with those obtained via route 1, one can say that they are much larger and that they have a higher dispersity. Moreover, the tendency to form Pb-rich intermetallic phases clearly increases with an increasing amount of $NaBH_4$. This experimental observation is in line with what one would expect; as the reduction potential of the Pb salt is much lower compared to that of the Pt salt, it is obviously much easier to reduce the Pt salt. In order to increase the amount of Pb in the intermetallic phase(s), a larger amount of reducing agent is required.

*3.1.2. Effect of Metal Salt Ratio on Size and Composition of Pt/Pb Nanoparticles.* In order to study whether the metal ratio in the nanoparticles can be controlled by the composition of the precursor microemulsions, w/o-microemulsions with different ratios of metal salts (Pt/Pb = 1:1, 1:2, and 1:3) were prepared and combined with a

**Table 3. *d*-Spacings from SAED Patterns and HRTEM Analysis of Sample 1c (13 mM $H_2PtCl_6$/13 mM $Pb(NO_3)_2$−0.012g $NaBH_4$)[a]**

| SAED | | | |
|---|---|---|---|
| *d*-spacings/nm | assignment (hkl) | *d*-spacings/nm | assignment (hkl) |
| 0.264 | $Pt/Pb_4$ (211) | 0.267 | $Pt/Pb_4$ (211) |
| 0.161 | $Pt/Pb_4$ (213) or Pt/Pb (103) | 0.209 | Pt/Pb (110) |
| 0.148 | $Pt/Pb_4$ (004), $Pt_3Pb$ (220), or Pt/Pb (202) | 0.183 | Pt/Pb (201) |
| 0.140 | $Pt_3Pb$ (220) or $Pt/Pb_4$ (332) | 0.163 | $Pt/Pb_4$ (213) or Pt/Pb (103) |
| 0.104 | | 0.147 | $Pt/Pb_4$ (004), $Pt_3Pb$ (220), or Pt/Pb (202) |

| HRTEM | |
|---|---|
| *d*-spacings/nm | assignment (hkl) |
| 0.359 | Pt/Pb (100) |
| 0.300 | Pt/Pb (101) |
| 0.224 | $Pt/Pb_4$ (202) or Pt/Pb (102) |
| 0.218 | Pt/Pb (102) |
| 0.211 | Pt/Pb (110) |

[a] SAED was measured in different areas of the sample (six different areas), and two different diffraction patterns were obtained.

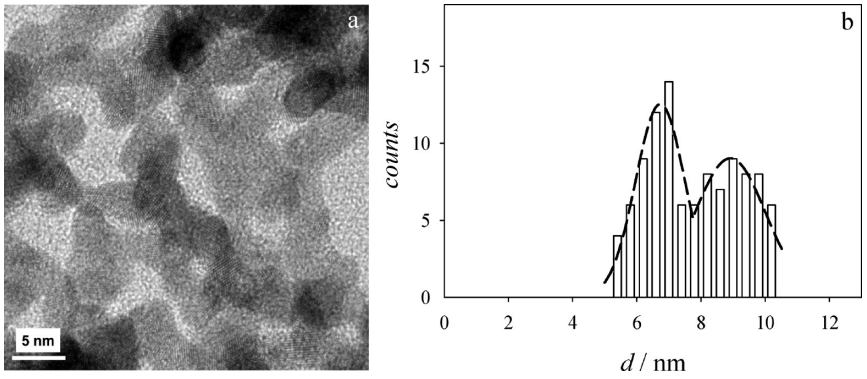


**Figure 3.** (a) HRTEM image of NPs and (b) size distribution of nanoparticles from sample 1c which indicates a bimodal distribution of particles with an average diameter of 6.5 ± 1.0 and 9.0 ± 1.5 nm (dashed line).

**Table 4. *d*-Spacings from SAED Patterns and HRTEM Analysis of Sample 1d (13 mM $H_2PtCl_6$/26 mM $Pb(NO_3)_2$−320 mM $NaBH_4$)**

| SAED | | | | | |
|---|---|---|---|---|---|
| *d*-spacings/nm | assignment (hkl) | *d*-spacings/nm | assignment (hkl) | *d*-spacings/nm | assignment (hkl) |
| 0.327 | | 0.391 | | 0.391 | |
| 0.238 | $Pt_3Pb$ (111) | 0.314 | $Pb_3O_4$ (220) | 0.314 | |
| 0.208 | Pt/Pb (110) or $Pt_3Pb$ (200) | 0.247 | Pb (200) | 0.247 | Pb (200) |
| 0.185 | Pt/Pb (201) | 0.229 | $Pt_3Pb$ (200) | 0.214 | Pt/Pb (102) |
| 0.172 | Pb (220) | 0.185 | Pt/Pb (201) | 0.148 | Pt/$Pb_4$ (004), $Pt_3Pb$ (220), or Pt/Pb (202) |
| | | 0.173 | Pb (220) | 0.127 | Pt/Pb (212), $Pt_3Pb$ (311), or Pt/$Pb_4$ (212) |
| | | 0.161 | Pt/$Pb_4$ (213) | | |

| HRTEM | |
|---|---|
| *d*-spacings/nm | assignment (hkl) |
| 0.319 | |
| 0.307 | Pt/Pb (101) |
| 0.246 | Pb (200) |
| 0.235 | $Pt_3Pb$ (111) |
| 0.217 | Pt/Pb (102) |

**Table 5. *d*-Spacings from SAED Patterns and HRTEM Analysis of Sample 1e (13 mM $H_2PtCl_6$/39 mM $Pb(NO_3)_2$−320 mM $NaBH_4$)**

| SAED | | HRTEM/nm | |
|---|---|---|---|
| *d*-spacings/nm | assignment (hkl) | *d*-spacings/nm | assignment (hkl) |
| 0.396 | | 0.318 | |
| 0.320 | | 0.308 | Pt/Pb (101) |
| 0.233 | $Pt_3Pb$ (111) | 0.222 | Pt/Pb (102) or Pt/$Pb_4$ (202) |
| 0.186 | Pt/Pb (201) | | |
| 0.175 | Pb (220) | | |
| 0.163 | Pt/$Pb_4$ (213) or Pt/Pb (103) | | |
| 0.145 | Pt/$Pb_4$ (004), $Pt_3Pb$ (220), or Pt/Pb (202) | | |
| 0.123 | Pt/Pb (212), $Pt_3Pb$ (311), or Pt/$Pb_4$ (212) | | |

w/o-microemulsion containing 320 mM of reducing agent (see samples 1b, 1d, and 1e in Table 1).

In sample 1d (13 mM $H_2PtCl_6$/26 mM $Pb(NO_3)_2$−320 mM $NaBH_4$), a metal salt ratio of Pt/Pb = 1:2 and the same amount of reducing agent as in sample 1b was used. SAED measurements of six different areas of the sample revealed the presence of Pt/Pb planes as well as planes of pure Pb and $Pt_3Pb$ as presented in Table 4. The HRTEM analysis shows the presence of Pt/Pb, $Pt_3Pb$, and Pb as can also be seen in Table 4. The EDX analysis shows some regions rich in Pb (Pt/Pb atomic ratio of 5:95) and other regions with a Pt/Pb atomic ratio around 2:1 (see Table S2 in Supporting Information). These results suggest that Pt/Pb NPs coexist with $Pt_3Pb$, Pt/$Pb_4$, and pure Pb.

Finally, sample 1e (13 mM $H_2PtCl_6$/39 mM $Pb(NO_3)_2$−320 mM $NaBH_4$) was prepared using a ratio of Pt/Pb = 1:3 and 320 mM of the reducing agent. SAED measurements of six different areas of the sample show the presence of planes that can be attributed to Pt/Pb, $Pt_3Pb$, and Pt/$Pb_4$ phases as presented in Table 5. The *d*-spacings determined by HRTEM analysis show the presence of (101) and (102) planes of the Pt/Pb phase. However, the crystal lattice with interplanar spacing of 0.222 nm can also be attributed to the (202) plane of Pt/$Pb_4$. The EDX analysis of sample 1e revealed some regions that are rich in Pb (Pt/Pb atomic ratio of 5:95) and other regions with an atomic ratio of Pt/Pb around 2:1 and 1:2, respectively. However, more regions with an atomic ratio of

Pt/Pb 1:2 rather than 2:1 were observed (see Table S2 in Supporting Information). These results once again suggest that the Pt/Pb NPs coexist with $Pt_3Pb$, $Pt/Pb_4$, and pure Pb NPs. In conclusion, one can say that the increase of the $Pb(NO_3)_2$ content increases the formation of the Pb-rich $Pt/Pb_4$ phase. Again, this result reflects the lower tendency of the Pb salt to be reduced compared to the Pt salt. It is an increasing concentration of either the reducing agent or the Pb salt, which leads to intermetallic phases with a larger Pb content.

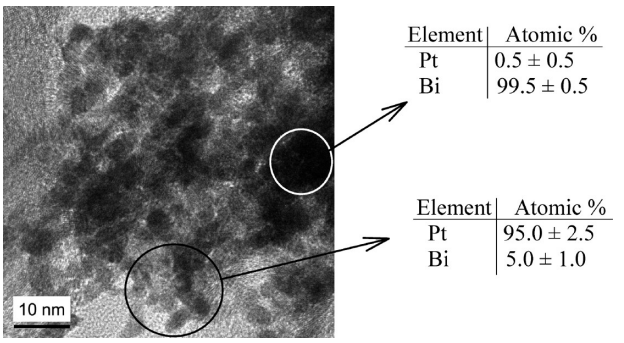


**Figure 4.** TEM image and EDX analyses of two different 5 $nm^2$ areas of the particles from sample 2a. The tables show the atomic percentage of Pt and Bi atoms detected by EDX in each marked circle.

**Table 6. *d*-Spacings from SAED Patterns and HRTEM Analysis of Sample 2a (13 mM $H_2PtCl_6$/13 mM $Bi(NO_3)_3$−160 mM $NaBH_4$ under $N_2$)**

| SAED | | | |
|---|---|---|---|
| *d*-spacings/nm | assignment (hkl) | *d*-spacings/nm | assignment (hkl) |
| 0.364 | | 0.226 | Pt (111) |
| 0.242 | Bi (104) | 0.195 | Pt (200) |
| 0.209 | Pt (220) | 0.139 | Pt (220) |
| 0.148 | Bi (122) | 0.118 | Pt (311) |

| HRTEM/nm | |
|---|---|
| *d*-spacings/nm | assignment (hkl) |
| 0.247 | Bi (104) |
| 0.232 | Bi (104 or/and 110) or Pt (111) |

**3.2. Pt/Bi Mixtures.** In order to prepare bimetallic Pt/Bi nanoparticles, the methods described in Section 2.2 were used. All particles presented in this section were prepared at $w_A = 0.08$, and a 1:1 metal salt ratio was used (13 mM $H_2PtCl_6$/13 mM $Bi(NO_3)_3$). A uniform dispersion of spherical nanoparticles was observed in all samples, and the TEM analysis of 60 particles selected randomly for each sample containing bismuth and platinum (Table 1) show that the average NP diameter is 4.5 ± 1.5 nm for all NPs prepared via route 1 (samples 2a and 2b). In the case of the particles prepared via route 2 (sample 2c), an average NP diameter of 6.5 ± 1.5 nm was observed. TEM images of particles from sample 2a (13 mM $H_2PtCl_6$/13 mM $Bi(NO_3)_3$−160 mM $NaBH_4$) are presented in Figure 4. The EDX analyses of two different regions in sample 2a (white and black circles in Figure 4) show that pure Pt, pure Bi, or the respective oxides were

**Table 7. *d*-Spacings from SAED Patterns and HRTEM Analysis of Sample 2b (13 mM $H_2PtCl_6$/13 mM $Bi(NO_3)_3$−320 mM $NaBH_4$ under $N_2$)**

| SAED | | HRTEM/nm | |
|---|---|---|---|
| *d*-spacings/nm | assignment (hkl) | *d*-spacings/nm | assignment (hkl) |
| 0.215 | Pt/Bi (110) | 0.306 | Pt/Bi (101) |
| 0.152 | Pt/Bi (202) | 0.224 | Pt/Bi (102) |
| 0.130 | Pt/Bi (211) | 0.207 | Pt/Bi (110) |

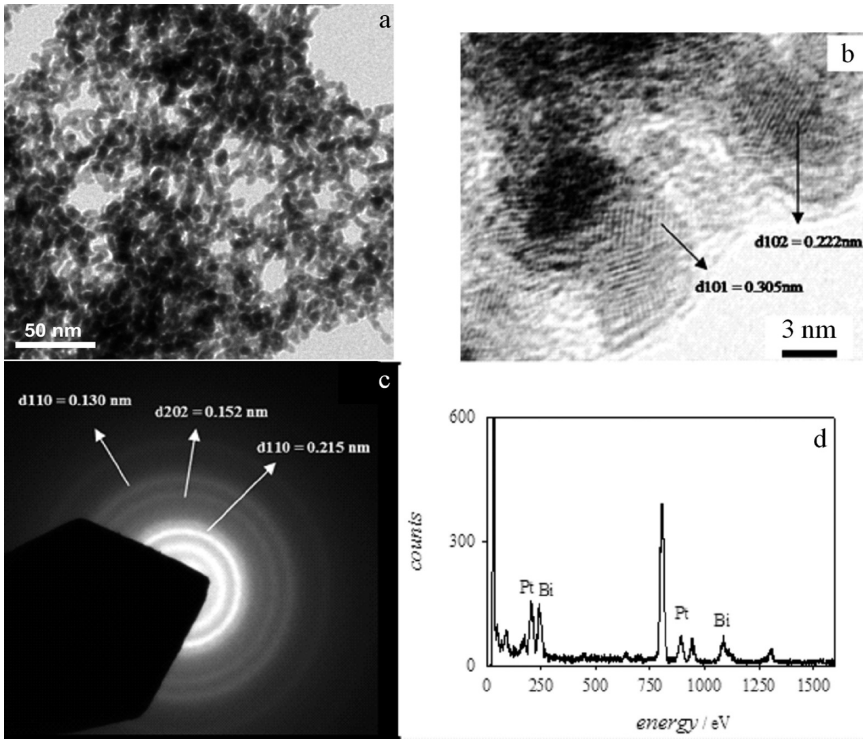


**Figure 5.** (a) TEM image and (b) HRTEM image of Pt/Bi nanoparticles from sample 2b. (c) Electron diffraction pattern of sample 2b. (d) EDX spectrum over 10 $nm^2$ area of sample 2b.

**Table 8. *d*-Spacings from SAED Patterns and HRTEM Analysis of Sample 2c (20 mM $H_2PtCl_6$/20 mM $Bi(NO_3)_3$−0.012g $NaBH_4$ under $N_2$)**

| SAED | | | |
|---|---|---|---|
| *d*-spacings/nm | assignment (hkl) | *d*-spacings/nm | assignment (hkl) |
| 0.364 | | 0.315 | |
| 0.289 | Pt/$Bi_2$ (210 cubic; 104 or 211 orthorhombic) | 0.243 | Pt/$Bi_2$ (220 cubic or 115 orthorhombic) or Bi (104) |
| 0.240 | Pt/$Bi_2$ (220 cubic or 115 orthorhombic) Bi (104) | 0.208 | Pt/$Bi_2$ (221 cubic or 025 orthorhombic) or $Bi_3Pt_2$ (202) |
| 0.208 | Pt/$Bi_2$ (221 cubic or 025 orthorhombic) | 0.147 | $Bi_3Pt_2$ (202) or Pt/Bi (202) |
| 0.178 | Pt/$Bi_2$ (230 cubic) or $Bi_3Pt_2$ (202) | 0.125 | $Bi_3Pt_2$ (212) or Pt/Bi (211) |
| 0.146 | $Bi_3Pt_2$ (202) or Pt/Bi (202) | | |
| 0.126 | $Bi_3Pt_2$ (212) or Pt/Bi (211) | | |

| HRTEM | |
|---|---|
| *d*-spacings/nm | assignment (hkl) |
| 0.325 | Pt/$Bi_2$ (021 orthorhombic) |
| 0.288 | Pt/$Bi_2$ (210 cubic; 104 or 211 orthorhombic) |
| 0.234 | Pt/$Bi_2$ (220 cubic or 115 orthorhombic) |

**Table 9. Compositions of Samples Used for the Synthesis of Pt/Pb and Pt/Bi NPs as well as the Crystal Structure and the Average Size of the NPs Obtained by HRTEM/TEM, SAED, and EDX Measurements[a]**

| Pt/Pb Nanoparticles | | | | |
|---|---|---|---|---|
| sample | Pt/Pb ratio metal salts | $NaBH_4$/mM | particle composition | NPs Size/nm |
| 1a | 1:1 | 160 | Pt/Pb, $Pt_3Pb$ | 4.0 ± 1.0 |
| 1b | 1:1 | 320 | Pt/Pb, $Pt_3Pb$, $Pt/Pb_4$ | 4.0 ± 1.0 |
| 1c | 1:1 | powder (0.012 g) | Pt/Pb, $Pt_3Pb$, $Pt/Pb_4$ | 7.7 ± 1.5 |
| 1d | 1:2 | 320 | Pt/Pb, $Pt_3Pb$, $Pt/Pb_4$ | 4.0 ± 1.0 |
| 1e | 1:3 | 320 | Pt/Pb, $Pt_3Pb$, $Pt/Pb_4$ | 4.0 ± 1.0 |
| Pt/Bi Nanoparticles | | | | |
| sample | Pt/Bi ratio metal salts | $NaBH_4$/mM | particle composition | NPs size/nm |
| 2a | 1:1 | 160 | Pt + Bi | 4.5 ± 1.5 |
| 2b | 1:1 | 320 | Pt/Bi | 4.5 ± 1.5 |
| 2c | 1:1 | powder (0.012 g) | $Pt/Bi_2$ | 6.5 ± 1.5 |

[a] See Table 1.

formed but no intermetallic phase (see Table S3 in Supporting Information). In contrast to the study of the Pt/Pb particles, we only varied the content of the reducing agent, while the ratio of the two metal salts was always kept constant.

In sample 2a, two diffraction patterns were found, as can be seen in Table 6. One diffraction pattern corresponds to the Pt phase, and the other shows *d*-spacings that can be attributed to the planes (122) and (104) of Bi and to the plane (220) of Pt. The *d*-spacings obtained by HRTEM analysis show the presence of the planes (104) or (110) of Bi and the plane (111) of Pt (Table 6). In order to optimize the process, a new route for the synthesis of Pt/Bi particles had to be found. One potential parameter to play with was the amount of the reducing agent. In samples 2b and 2c, the synthesis of NPs was carried out at higher concentrations of reducing agent and under nitrogen atmosphere (see Table 1).

In sample 2b (13 mM $H_2PtCl_6$/13 mM $Bi(NO_3)_3$−320 mM $NaBH_4$ under $N_2$), the synthesis of the metallic nanoparticles was carried out under nitrogen atmosphere and a concentration of 320 mM $NaBH_4$ was used. A TEM image of the particles is shown in Figure 5a. By HRTEM analysis, the planes (101), (102), and (110) of the Pt/Bi phase were observed, as can be seen in Figure 5b and in Table 7. Identical diffraction patterns were obtained by SAED analysis from six different areas. The electron diffraction pattern of sample 2b shows the presence of the planes (110), (202), and (211) of the Pt/Bi phase (see Figure 5c and Table 7). The EDX analysis confirmed that the atomic ratio of Pt/Bi was 1:1 over the whole sample (Figure 5d) even in areas smaller than 5 $nm^2$ (see Table S3 in Supporting Information). These results suggest that the Pt/Bi nanoparticles are a single, ordered Pt/Bi intermetallic phase rather than a mixture of two monometallic nanoparticles as observed for sample 2a.

Finally, sample 2c was prepared by adding 0.012 g of $NaBH_4$ as a powder to a w/o-microemulsion containing 13 mM $H_2PtCl_6$ and 13 mM $Bi(NO_3)_3$ under nitrogen atmosphere (route 2). The EDX analysis of sample 2c (see Table S3 in Supporting Information) shows the presence of regions with different atomic ratios of Pt/Bi. Some regions have an atomic ratio of Pt/Bi around 1:2 and others around 3:2, respectively. In Table 8, the *d*-spacings determined by SAED and HRTEM analysis indicate the presence of at least five planes that correspond to the $Pt/Bi_2$ phase. These results suggest that the nanoparticles are an ordered $Pt/Bi_2$ phase rather than a mixture of two

monometallic nanoparticles, as observed in sample 2a. However, the formation of pure Pt or Pt oxides cannot be discarded as not all Pt atoms were consumed for the formation of the $Pt/Bi_2$ phase.

On the basis of the SAED data, the simultaneous formation of Pt/Bi and $Pt_2Bi_3$ cannot be ruled out although the amounts are expected to be very low. In conclusion, one can say that it is only above a certain $NaBH_4$ concentration that intermetallic phases are formed. Once this concentration is reached, very pure phases rather than mixtures of different phases are formed. Adding the $NaBH_4$ as a solid leads to the formation of the Bi rich phase $Pt/Bi_2$, which is in agreement with the observations made for Pt/Pb. The main difference between the Pt/Pb and the Pt/Bi systems is the fact that in the case of Pt/Bi one main compound is formed, while for Pt/Pb mixtures different intermetallic phases are favored.

## 4. Conclusions

The synthesis of Pt/Pb and Pt/Bi intermetallic nanoparticles was successfully achieved using the microemulsion method. The size of the particles was roughly 6 times smaller than the size of the w/o-microemulsion containing the metal salt and reducing agent as observed by SAXS. An extensive study on the influence of the water content $w_A$ will follow in a future publication. In case of Pt/Pb NPs, the effect of the Pt/Pb metal salt ratio and of the amount of the reducing agent on the particle size and composition was studied. The results revealed that the formation of the Pb-rich $Pt/Pb_4$ phase is favored in the presence of high $NaBH_4$ concentrations and/or at high $Pb(NO_3)_2$ content. On the other hand, the synthesis of intermetallic Pt/Bi particles was only possible at high enough concentrations of $NaBH_4$ in the w/o-microemulsion ($w_A = 0.08$). At a concentration of 160 mM $NaBH_4$, only pure or oxidized Pt particles plus pure or oxidized Bi particles were obtained. Increasing the concentration of $NaBH_4$ from 160 to 320 mM led to the formation of a single intermetallic Pt/Bi phase. Addition of solid reducing agent to the w/o-microemulsion containing the metal salts led to the formation of an intermetallic $Pt/Bi_2$ phase. The formation of $Pt/Bi_2$ nanoparticles was also reported by Xia et al.[32] who used polyvinylpyrrolidone (PVP) dissolved in HCl to synthesize $Pt/Bi_2$ nanoparticles and added the solid reducing agent to the system (our route 2). According to Okamoto,[33] the formation of a 1:1 Pt/Bi intermetallic phase is less favorable than the formation of $Pt/Bi_2$ phase. Currently, an extensive MC simulation is being carried with the aim to better understand the experimental results. However, we can conclude that following route 1 (mixing two microemulsions) led to the formation of a single intermetallic Pt/Bi phase, while following route 2 (adding solid $NaBH_4$) led to the formation of an intermetallic $Pt/Bi_2$ phase. It could not be clarified yet whether this is caused by the different total amounts of $NaBH_4$ or by the different reducing routes. Finally, it has to be mentioned that in both cases the addition of solid $NaBH_4$ led to larger particles compared to the addition of a reducing microemulsion. All results are summarized in Table 9.

**Acknowledgment.** L.M.M. and C.S. would like to thank the Science Foundation Ireland (SFI). All authors are grateful for the financial support provided by the European ESTEEM programme (European Union, FP 6, Integrated Infrastructure Initiative, Reference 026019).

**Supporting Information Available:** SAXS data of the microemulsions as well as EDX data of the nanoparticles (PDF). This material is available free of charge via the Internet at http://pubs.acs.org.

(32) Xia, D.; Chen, G.; Wang, Z.; Zhang, J.; Hui, S.; Ghosh, D.; Wang, H. *Chem. Mater.* **2006**, *18*(24), 5746–5749.
(33) Okamoto, H. *J. Phase Equilib.* **1991**, *12*(2), 207–210.
(34) Holmberg, K. *J. Colloid Interface Sci.* **2004**, *274*(2), 355–364.
(35) Schmidt, J.; Guesdon, C.; Schomäcker, R. *J. Nanopart. Res.* **1999**, *1*(2), 267–276.